DIAGNOSTIC INVESTIGATION OF EXCESSIVE CAMBER IN PRESTRESSED SLAB UNITS

FLORIDA DEPARTMENT OF TRANSPORTATION
M. H. ANSLEY STRUCTURES RESEARCH CENTER
WRITTEN BY: ARIANA MORALES RAPALLO
REVIEWED BY: CHRISTINA FREEMAN, P.E.
2020

Table of Contents

Introduction

In May 2018, six (6) Prestressed Slab Units (PSU) were rejected from a bridge construction project due to high camber. Four (4) of these slabs have dimensions of 12 in. x 48 in. x 48 ft -11 in. and two (2) of them have dimensions of 12 in. x 48 in. x 48 ft. On December 12th, 2018, the FDOT M.H. Ansley Structures Research Center accepted these six slabs to be stored in their facility. RS&H, serving as Construction Engineering Inspector (CEI) for the project, asked FDOT to evaluate why the slabs experienced a higher camber than predicted and higher than similar slabs on the same project. All slabs for the project were cast and pretensioned at the same precast facility and during the same time of the year.

The objective of this research was to evaluate and test different hypotheses regarding the cause of excessive camber on the six slabs rejected. The hypotheses were established based on calculations, measurements, and drawings. An experimental test was required to verify the information provided in both plans and construction documents of the slabs. The hypotheses reviewed in this project are listed below:

Hypotheses

- Failure in reporting an excess of force in the strands' pretensioning process could have caused a higher load transfer to the slab and therefore a higher camber was produced.
- The design required that four prestressing strands in the bottom layer of strands were debonded, two of them for 8 ft and two of them for 4 ft. If the debonded length was shorter than stated in the plans, then a longer effective length is applied and therefore higher prestress load is acting on the slab.
- Concrete properties (compressive strength, f_c', initial modulus of elasticity, E_{ci}, and unit weight, w_c) may have been different than what was assumed for design, resulting in a higher camber than predicted.
- Excessive compressive stress could have caused micro-cracking and a reduced moment of inertia, leading to excessive camber.
- Thermal gradient due to solar effects could have caused camber in some slabs to be excessive.

Literature Review

Prestressed concrete bridge girders and slabs have been widely used for roads and highways around the country, however, design for and prediction of camber have historically been difficult for prestressed products. Camber is upward deflection created by the application of axial forces placed with an eccentricity from the neutral axis of the girder and its purpose is to counteract the downward forces created by self-weight of the member and service loads (Cook, Bloomquist, Sanek, & Ansley, 2005). According to Yazdani et al., FDOT has experienced deck casting problems in the field due to unexpected camber. In fact, it is stated by Yazdani et al. that large AASHTO girders don't experience camber as fast as smaller girders during the first month after casting. However, they found the actual measured camber in all girders was still higher than the FDOT predictions (1999). Although the shape of the member has an influence on camber, some of the most important variables for camber in prestressed girders and slabs are the material properties such as compressive strength, modulus of elasticity, and amount of creep and shrinkage (Storm, Rizkalla, & Zia, 2013). Several methods exist to calculate camber and long-term prestressed losses in prestressed concrete members, and they will be discussed.

The camber calculated in the design and the camber experienced in the field are not always the same because of internal and external factors. The camber in pretensioned concrete members depends on several aspects, for instance, component properties such as strength, type, quality, and stiffness directly affect the modulus of elasticity (Tadros, Al-Omaishi,, Seguirant, & Gallt, 2003). The strength of the concrete plays an important role in the camber prediction, in fact, an insufficient tensile strength at the time of release could yield cracks due to the high tensile forces at the negative moment region, when the member deflects upwards (Yazdani, Mtenga, & Richardson, 1999). It is typically assumed that the time for the prestress transfer is one day, however, in some cases, fabricators let the concrete cure over the weekend and then apply the prestress forces. This might cause a false prediction of the camber since the modulus of elasticity and strength of the concrete are higher than first calculated (Storm, Rizkalla, & Zia, 2013).

Shrinkage and creep are two physical processes which the concrete goes through when hardening and resisting sustained load, respectively, and they both could affect the final camber of the concrete member. Shrinkage is the change in concrete volume with time in an unstressed condition (Cook, Bloomquist, Sanek, & Ansley, 2005). Many variables can affect shrinkage such as water-to-binder ratio, curing practices, relative humidity of the environment, ambient temperature, aggregate properties, and size and shape of the concrete element. Shrinkage is influenced by the aggregate stiffness because the aggregate restrains the shrinkage of the paste (Tadros, Al-Omaishi,, Seguirant, & Gallt, 2003). Creep is defined as the increase in strain with time under sustained stress conditions (Cook, Bloomquist, Sanek, & Ansley, 2005). The creep not only depends on time and applied load but also on volume content of hydrated cement paste, ambient relative humidity, type and volume of aggregates, age of concrete at the time of loading, stress level, and the geometry of the member. The size of the member highly influences the magnitude of creep, in fact, the magnitude of creep observed in larger members is significantly lower than in small members, based on a study which examined concrete cylinders from 4 to 24 inches in diameter and I-shape members from 11.5 to 46 inches in height (Tadros, Al-Omaishi,, Seguirant, & Gallt, 2003). Additionally, extra curing time of the concrete can affect creep since it is sensitive to the strength of the concrete at the time of prestress transfer (Storm, Rizkalla, & Zia, 2013). The prestress losses of a concrete member depend in part on the creep experienced. Both creep and shrinkage grow logarithmically over time and this growth is proportional

to an increase in long-term camber, with creep increasing long-term camber and shrinkage decreasing it (Cook, Bloomquist, Sanek, & Ansley, 2005) (Nawy, 2005).

Relaxation of the strands can also affect the camber of the structural member. When the steel prestressing strands are stressed and held at constant strain, the stress will decrease over time; this is an effect called intrinsic relaxation loss. This loss is larger with higher stress and higher temperature. However, most current steel strands used now are "low-lax," which decrease the relaxation loss and therefore the prestress loss due to relaxation is very small (Tadros, Al-Omaishi,, Seguirant, & Gallt, 2003). Thermal expansion of the strands can also affect the prestressing forces. Prior to the prestress transfer and during the concrete curing process, the temperature in the strands can increase due to the cement hydration process. This can cause a reduction of the prestressed force as much as 11%. However, a portion of the force is regained after six to eight hours due to the bond between steel and concrete ending with a total loss of approximately 6% (Storm, Rizkalla, & Zia, 2013).

Thermal gradient due to solar effects can influence the camber in the structural member and the camber is observed to be related to the depth of the member, with heating in areas exposed to the sun and cooling in shaded areas (Storm, Rizkalla, & Zia, 2013). When there is a thermal gradient in the concrete member, which means cool and hot areas at the same time affecting the concrete, it can create expansion, usually at the top due to the sun, and contraction at the bottom due to the shade. These simultaneous movements can cause changes in the camber.

Since camber is the result of two major effects in opposite directions: negative moment due to prestressing and positive moment due to self-weight, the prediction of it cannot be expected to be exact. There are two design specifications commonly used by engineers in the U.S. to predict camber as accurately as possible. The 2010 AASHTO LRFD Bridge Design Specifications (2017) provides a method to estimate creep, shrinkage, and prestress losses, however, it does not provide a procedure to calculate the final camber (Storm, Rizkalla, & Zia, 2013). The PCI Design Handbook: Precast and Prestressed Concrete (2010) provides a method to estimate the loss of prestressing as well as a simplified procedure to calculate camber using multipliers. These multipliers account for creep effect due to sustained loads and are suitable for building designs, however, Yazdani et al. state more details may be needed for bridge designs to account for environmental conditions and time-dependent factors (1999). The PCI Bridge Design Manual recommends using the multipliers with caution since they only provide a "reasonable estimate of camber at the time of erection" and "the method does not properly account for the significant effects of a large cast-in-place deck". Additionally, the PCI Bridge Design Manual advises designers that "the prestressing levels should not be increased in order to reduce or eliminate long-term downward deflection that might be predicted if the given multipliers are used" (Storm, Rizkalla, & Zia, 2013). FDOT's Structures Design Office developed a software, FDOT LRFD Prestressed Beam Program, to design and review simply supported pre-tensioned girders. It considers material properties, creep and shrinkage, as well as environmental effects on prestress losses in concrete. In early versions of the program, the factors for prestress losses were based on ACI Committee 209 (2015) recommendations (Yazdani, Mtenga, & Richardson, 1999). The Prestressed Beam program was modified in 2005 based on the University of Florida research called "Field Verification of Camber Estimates for Prestress Concrete Bridge Girder" done by Cook et al. (2005) and the creep factors in the programs were modified following the current AASHTO LRFD guidelines (2017).

Regarding prestress losses in pretensioned concrete members, there are several experimental methods: monitoring concrete strain, determining initial crack and crack re-opening loads, cutting the prestressing reinforcement, and inducing a crack with a hole drilled in the bottom flange of a member (Martí-Vargas, Garcia-Taengua, & Caro, 2014).

In the research conducted by Marti-Vargas et al. (2014), a methodology for testing prestressed reinforcement was developed. It is called the ECADA test method and evaluates the bond length and the changes in length through time. This method works by "characterizing the bond by release and pull out". It requires instrumentation to measure prestressing reinforcement forces, displacement transducers to measure the slip at the ends, and strain gauges to obtain the longitudinal concrete surface strain profile. In the project by Marti-Vargas et al., several specimens were cast with different embedment lengths under the same conditions of pretensioning. The authors concluded that the technique provides additional knowledge about the bond behavior and prestress losses, additionally, a better determination of transmission and anchorage length and available prestress force in different cross-sections of the member.

On the topic of effective prestress, research was done by Pessiki et al. (1996) titled *Evaluation of Effective Prestress Force in 28-year-old Prestressed Concrete Bridge Beams*. They determined the effective prestress force in two full-scale beams after 28 years of service. The beams belonged to the Pennsylvania Department of Transportation and were tested by the Center for Advanced Technology for Large Structural System at LeHigh University. The methodology to evaluate the prestressing forces on the beam was the "Cracking Load Test" and the "Decompression Load Test". The experimental testing was divided into three different phases. First, the load was applied until the first cracks were created and the researchers then applied the strain gauges and displacement transducers around the crack. The second phase consisted of loading the beam again and determining the decompression load based on the strain vs load graph after re-loading. This load was determined by the point where the slope changes and decreases. If this point is not noticeable, then trendlines were added in the two regions of the graph and the intersection of them is assumed as the decompression load. Finally, the last phase consisted of overloading the beams until failure. Once the decompression load was obtained, the prestress force on the strands was calculated and therefore the effective prestress force.

Similarly, research conducted by Hamilton et al. (2009) titled *Determination of Service Stresses in Pre-tensioned Beams* from the University of Florida involved two inverted tees with the objective to determine the cracking behavior in prestressed concrete girders as well as the calculation of the cracking moment. Hamilton et al. followed the Pessiki et al. procedure to determine the effective prestress in both girders. They defined the decompression load as the average load where the strain vs load curve, for all the strain gauges installed at the bottom of the girder adjacent to the first crack, reached a plateau. The theoretical definition of the decompression load is the load required to reach a zero stress at the tension fiber of the member. Additionally, they calculated the cracking moment using two methods: the first method was by experimentally calculating the modulus of rupture of concrete, f_r, and defining the cracking moment as the amount required to cause the net tensile stress equal to f_r. The second method consisted in similar calculations but using concrete strength to calculate the modulus of rupture using $f_r = 7.5\sqrt{f'c}$.

In research conducted by Azizinamini et al. (1996) titled *Application of a New Nondestructive Evaluation Technique to a 25-Year-Old Prestressed Concrete Girder* a new nondestructive technique to evaluate the available stress in the girder was proposed. This new technique is based on the stress state around a cylindrical hole drilled at the bottom of the girder. By drilling a hole at the bottom flange, a control crack

is induced parallel to the girder. Once the crack is created, lateral pressure was applied to close the crack and it was identified as the pressure where the force normal to the crack is zero. Azizinamini et al. (1996) evaluated the proposed non-destructive method with comparison to a crack opening test. It was concluded that the proposed non-destructive method was promising as a new method of effective prestress evaluation.

The compressive stress at release in prestress girders is limited by code when designing prestressed concrete girders. Excessive compressive stress at release could affect the girder by causing cracking in the tensile fiber, excess camber, concrete splitting at the ends, among other affects. In research conducted by Dolan and Krohn (2007) titled *A Case for Increasing the Allowable Compressive Release Stress for Prestressed Concrete*, they conducted two surveys to evaluate the compressive transfer stresses. They concluded that the limit for compressive stress at release should be increased to $0.7f_c'$ based on support from previous research and precaster and industry response to a survey. However, they stated that camber and prestress losses are more variable when the compressive stresses are higher and therefore, they suggest that a camber prediction and prestress loss calculation should be refined in cases of higher compressive transfer stress. Moreover, in their survey they found that in some cases when the compressive stress is greater than $0.75f_c'$, there was deck cracking, minor stress crack at the ends, short horizontal cracks, and the greater the compressive transfer stress the more cracking at the tensile zone was noted, including cases without an increased tensile stress. Additional research by Castro et al. (2004) found that in all cases studied, the camber increased with an increase in compressive stress release. They stated that the increase in camber only depended on the compressive stress release and not on the cross-section geometry or type of concrete.

Project Background

Project Information

From February 2018 to March 2018, fifty-seven (57) PSU slabs were cast for the bridge project in Florida and only six (6) of them were rejected three months later due to high camber. The rejected slabs were marked as BS 2-02 JC-9, BS 2-02 JC-10, BS 2-02 JC-11, BS 2-02 JC-12, BS 2-06 JC1-13 and BS 2-06 JC-14. The slabs JC-09, JC-10, and JC-11 were cast on February 1 and the slabs JC-12, JC-13, and JC-14 were cast on February 13. The concrete strength measured at release was, on average, 5400 psi and increased to an average of 8365 psi for both mixes at 28 days. The concrete mix used for the slabs BS 2-02 JC-12, BS 2-06 JC1-13, and BS 2-06 JC-14 cast on 02/13/18 had 4.9% air content, a spread of 29 in., and the slabs were released at 3 days old. The concrete mix used for slabs BS 2-02 JC-9, BS 2-02 JC-10, and BS 2-02 JC-11 cast on 02/14/19 had 4.8% air content, a spread of 25 in., and the slabs were released at 2 days old. In Table 1, the material used for the concrete mix of the rejected slabs is shown based on the information provided by the precaster.

Table 1 Concrete Material Components

Material	*Product*
Coarse Aggregate	67 Rock
Pozzolanic Material	Fly Ash
Cement	Type I, II
Admixtures	Air-Entraining Admixture
	Set Retarding Admixture
	High Range Water Reducing Admixture

The slabs were designed to have three layers of prestressing strands. The bottom layer consisted of twenty-six (26), 0.6 in. diameter, 270 ksi lo-lax strands stressed to 43.94 kips. The distance from the bottom of the slab to the centroid of the bottom layer of strands was 3 in. Two (2) were debonded 8 ft from the ends and two (2) were debonded 4 ft from the ends. A second layer 5 in. from the bottom of the slab with six (6), 0.6 in. diameter, 270 ksi lo-lax strands were also stressed to 43.94 kips each. Finally, a top layer with four (4), 0.375 in. diameter, 270 ksi lo-lax strands were located 3 in. from the top of the slabs and stressed to 10 kips each. In Figure 1, the strand location and slab details are shown.

According to the prestress tensioning report provided by the precaster, the strands in the bottom layers were tensioned to an average of 44.33 kips with an elongation of 33.25 in. The ambient temperature at the tensioning was around 80 degrees Fahrenheit.

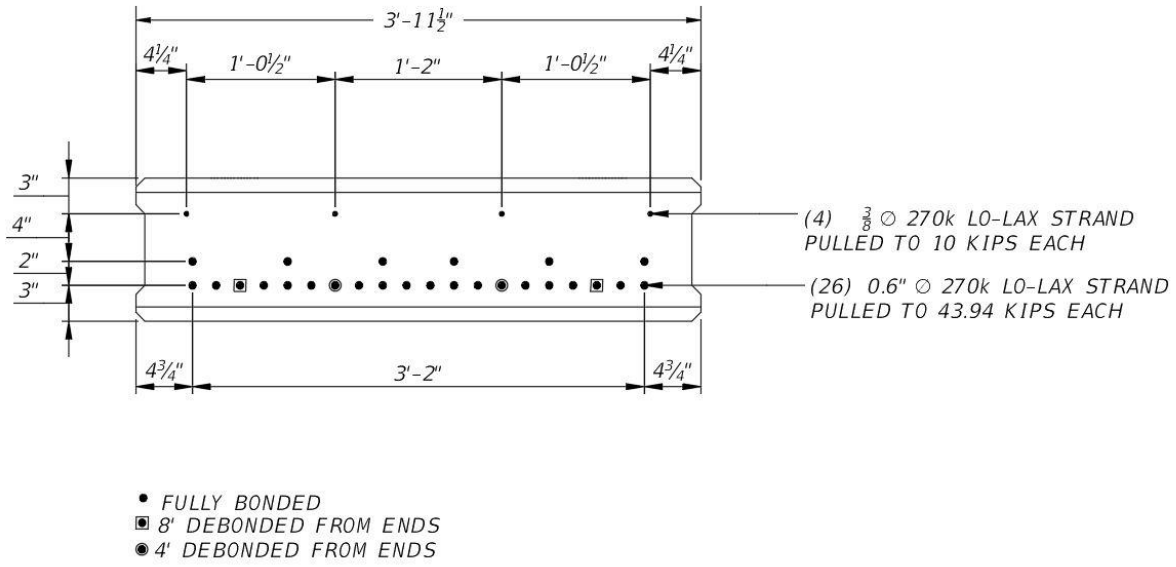

Figure 1 PSU Cross-Section

Per bridge construction plans, the predicted cambers were 1.245 in. (BS2-02) and 1.337 in. (BS2-06) at 120 days. After the slabs were cast, the camber was measured four times by the precaster. The first reading was a little less than a month after the concrete was cast and the last reading was three months after the concrete was cast. The camber readings in the six (6) rejected slabs varied from 4 in. to 4.75 in., as can be seen in Table 2.

Table 2 Camber Measurement

Mark #	*Serial #*	*Cast Date*	*Camber (in.) on 3/8/2018*	*Camber (in.) on 3/14/2018*	*Camber (in.) on 4/16/2018*	*Camber (in.) on 5/16/2018*
BS2-02	JC 9	2/14/2018		4.25	4.25	4.375
BS2-02	JC 10	2/14/2018	4.375	4.375	4.25	4.5
BS2-02	JC 11	2/14/2018	4.25	4.25	4.125	4.125
BS2-02	JC 12	2/13/2018	4.0	4.0	4.125	4.0
BS2-06	JC 13	2/13/2018		4.375	4.375	4.75
BS2-06	JC 14	2/13/2018		4.0	4.0	4.0

Analysis of Camber from Project Information

The rejected slabs were compared to the accepted slabs from the project to investigate any difference in the temperature at casting, the temperature at release, relative humidity and the strength of the concrete at release that might have caused the excess camber. This information was obtained from readings made by the precaster and public weather records and Figures 2-5 show the relationship between the accepted and rejected slabs for temperature, relative humidity, and concrete strength.

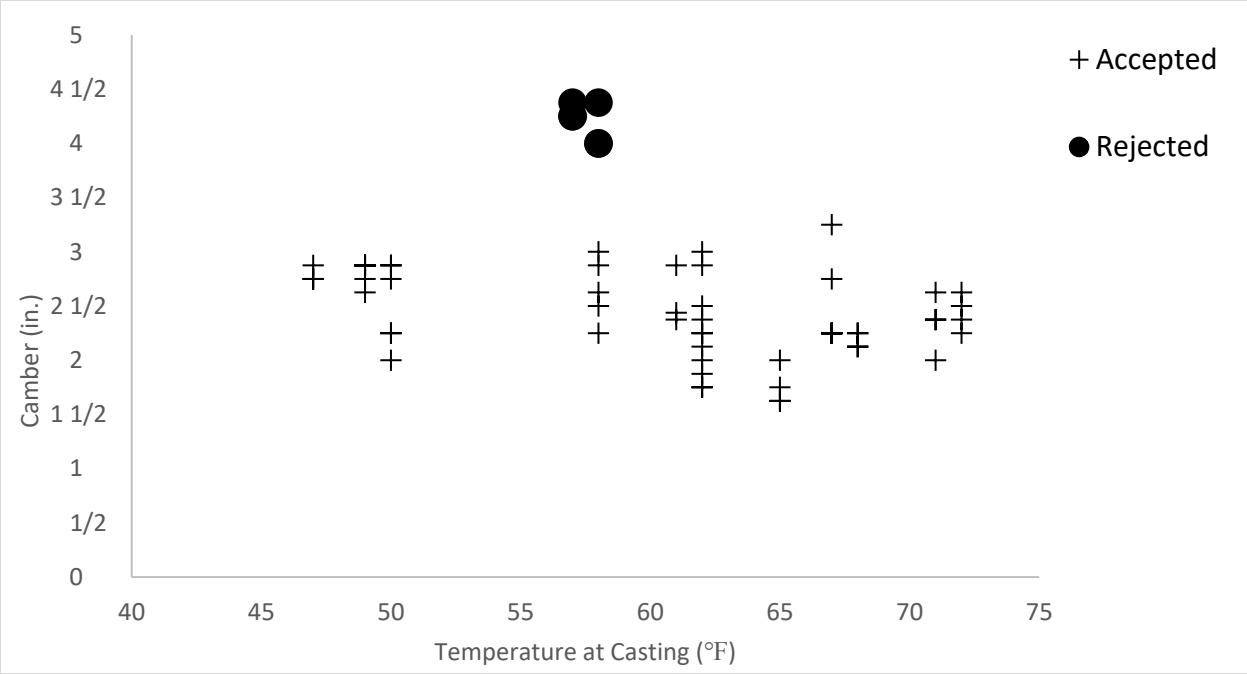

Figure 2 Camber vs Temperature at Casting

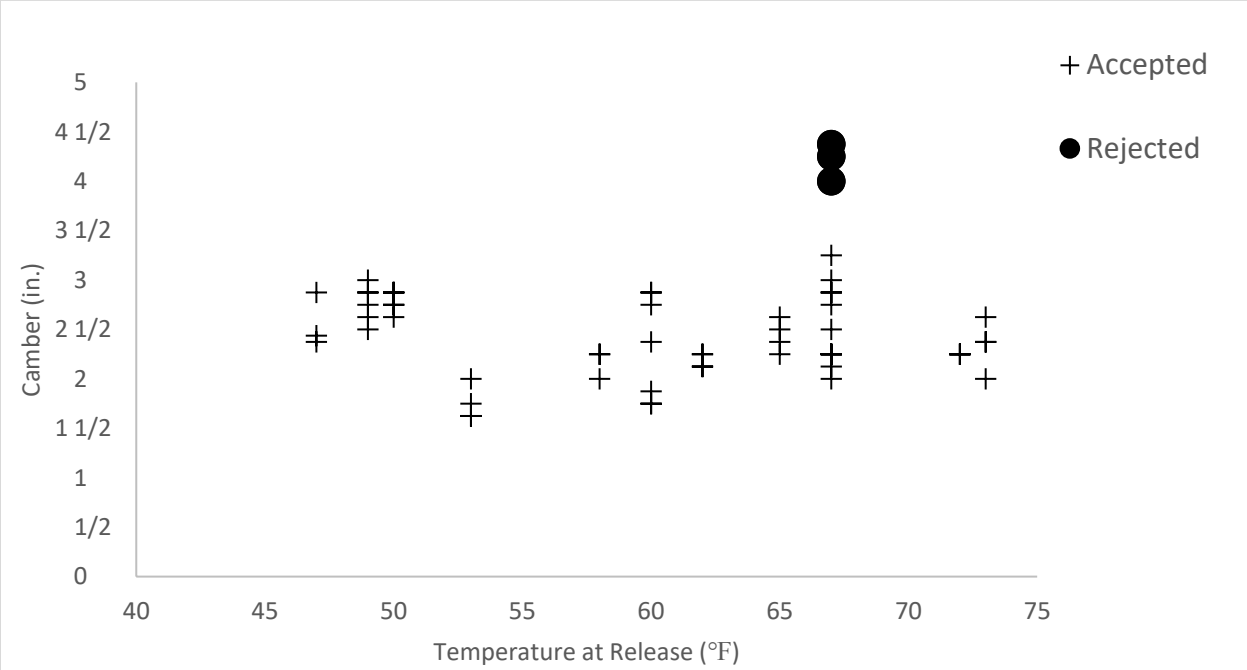

Figure 3 Camber vs Temperature at Release

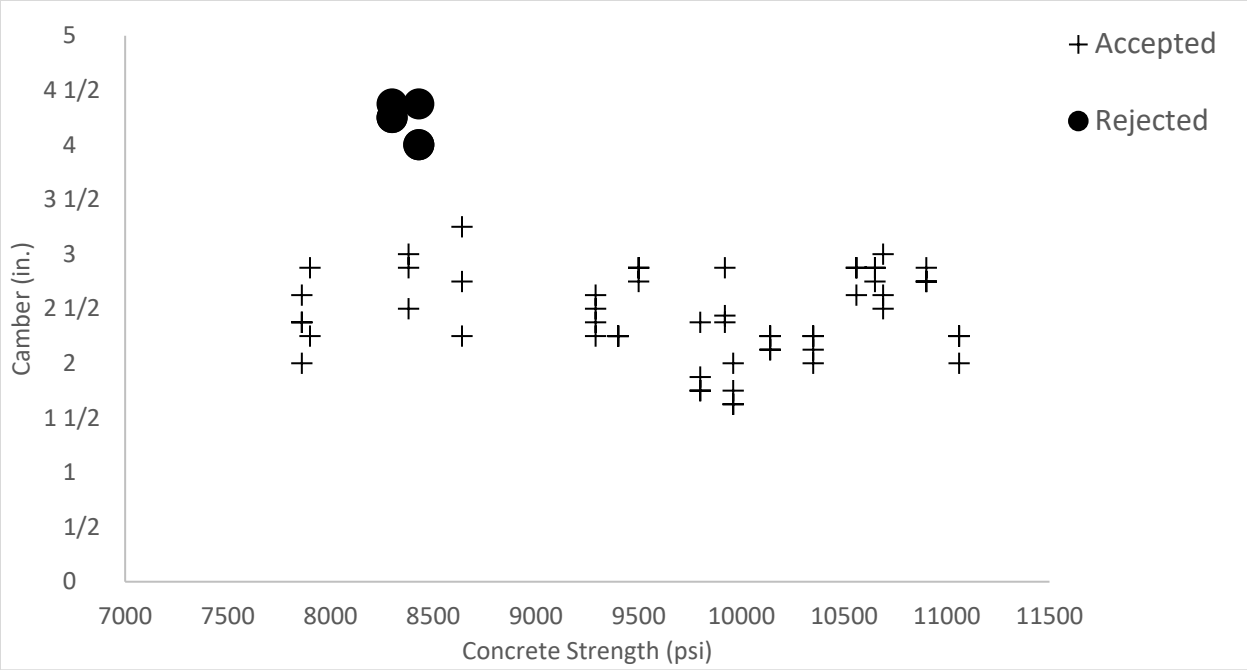

Figure 4 Camber vs Concrete Strength at Release

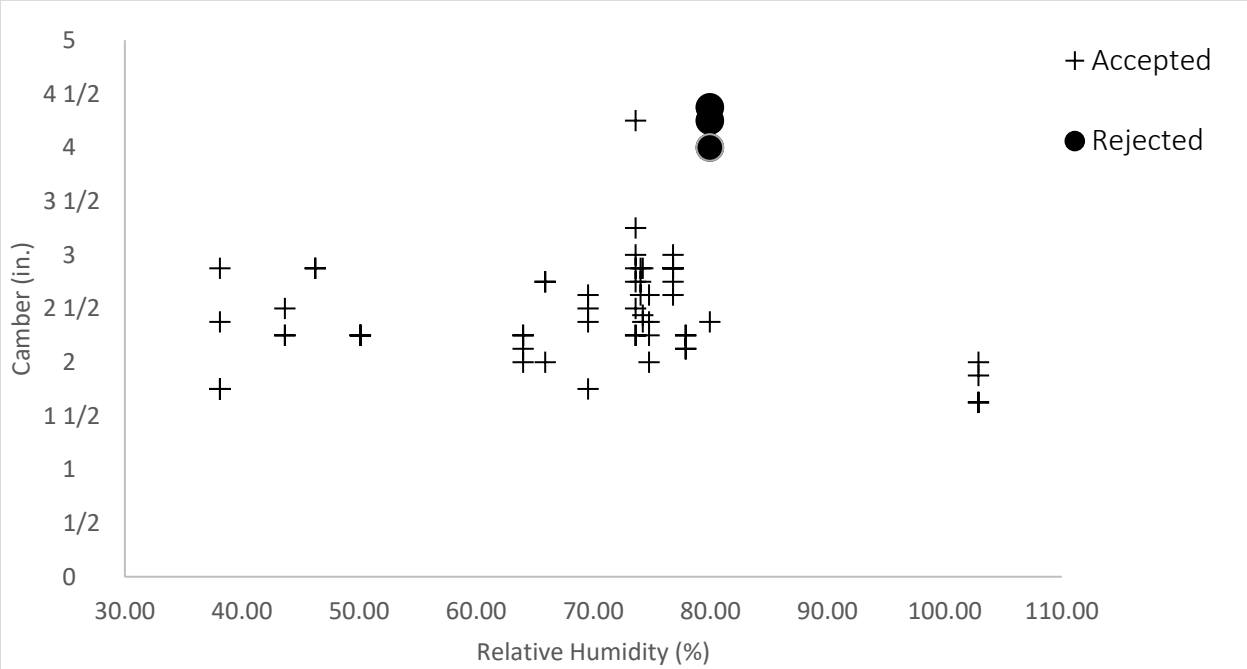

Figure 5 Camber vs Relative Humidity

As can be seen in Figure 2, the temperature at casting for the rejected slabs is between 55 to 60 degrees Fahrenheit, which is approximately the average of the casting temperatures of accepted slabs in the project.

However, the temperature at release in Figure 3 for the rejected slabs is located in the higher temperature range, between 60 and 75 degrees Fahrenheit, compared to the accepted slabs. It is important to mention that this temperature corresponds to the average temperature of the day, however, the exact temperature at casting time and release time are unknown. In Figure 4, the concrete strength at release of the rejected slabs corresponds to the lower range of the accepted slabs, yet, a high number of accepted slabs are in the low range of concrete strength between 5000 psi and 7000 psi at release. Since relative humidity can affect creep and shrinkage it was important to evaluate this variable at casting. As shown in Figure 5, the relative humidity present when the rejected slabs were cast is within the range of all slabs cast in the project.

Precast Slab Storage

To evaluate the possibility of a thermal gradient affecting camber in the rejected slabs during the storage period, pictures from the precast yard were requested from the project's CEI. The slabs were stored on top of each other as can be seen in Figure 6 and Figure 7. The four slabs shown in Figure 6 are all marked as slab type BS2-02. All four were 48 ft - 11 in. long and were rejected for high camber. As can be seen in Figure 6, the slabs were exposed to thermal effects unequally, with the lower slabs shaded. But, all four slabs had similar, unacceptably high camber.

Figure 6 Slab Storage at the Precast Yard, Overall View

Figure 7 Slab Storage at the Precast Yard, End View

Observation

Camber Measurement

Over several months, while the Prestressed Slab Units (PSU) were stored at the FDOT SRC, weekly camber readings were taken using a ZipLevel Pro 2000 for the six rejected slabs. The ambient and concrete temperature were recorded as well to analyze the effect of temperature on the camber of the slabs. These readings were used to measure the effect of temperature in the slabs and the camber change in a non-destructive way. The slabs were stored on two concrete beams supports with a constant span length of 42 ft behind the FDOT Structure Research Center building. As shown in Figure 8, slabs JC-9, JC-10, JC-11, JC-12, and JC-14 were stored from east to west whereas slab JC-13 was oriented from north to south.

Figure 8 PSU Slab Storage

The camber readings seem to be consistent throughout the measurements, with a maximum change of 9% and the same behavior for all slabs. In the camber readings, time, ambient and concrete temperatures are shown for five different measurements throughout 2 months for the six slabs. Additionally, the camber was measured one last time when the slabs were placed on the supports just before being tested (JC-10, JC-11, JC-12, JC-14). It is important to note that these last readings were done inside the lab with a span length of 46 ft, which closely matches the storage conditions at the precast yard. The higher camber observed during storage at the FDOT SRC is likely due to the shorter support distance of 42 ft.

Table 3 Camber Readings

Date	*Time*	*Ambient Temp. (°F)*	*Concrete Temp. (°F)*	*JC-9*	*JC-10*	*JC-11*	*JC-12*	*JC-13*	*JC-14*
8/12/2019	9:00 AM	83	85	5.25	5.40	5.00	5.05	5.60	4.95
8/19/2019	9:20 AM	84	84	5.40	5.45	5.40	5.40	5.60	5.00
8/26/2019	9:00 AM	79.6	79	5.45	5.20	5.10	5.15	5.50	4.85

9/3/2019	10:00 AM	80.6	88	5.50	5.45	5.00	5.20	5.85	5.10
9/11/2019	8:10 AM	73.4	78	5.10	5.30	5.00	5.20	5.40	4.85
10/3/2019	8:20 AM	73.4	73.6	5.25	5.10	4.90	5.05	5.30	4.80
02/06/2020				N/A	4.52	4.55	4.83	N/A	4.25

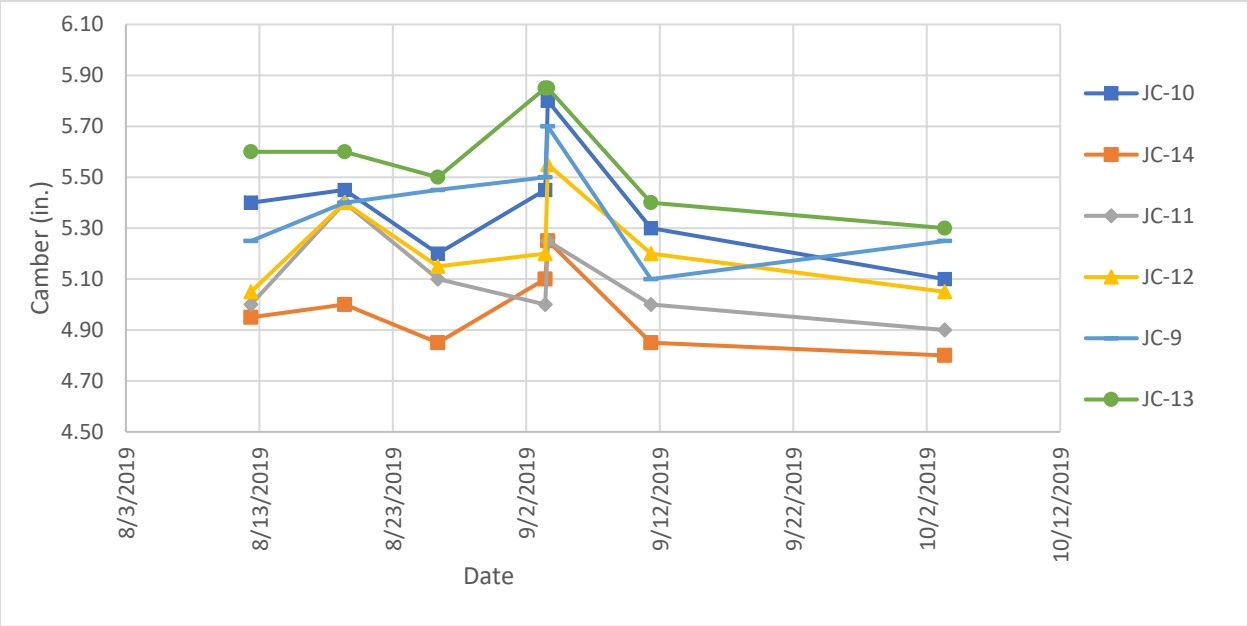

Figure 9 Camber Readings

As can be seen in Figure 9, all the slabs experienced similar camber changes throughout the measurement period. When the ambient and concrete temperatures were high the camber tended to be high. The readings during these two months showed a higher camber than what was measured at the precast plant when the slabs were rejected in May 2018, shown in Table 2. The primary reason for the difference is assumed to be the shorter span length during storage at FDOT SRC.

Crack Documentation

Cracks were visually identified and mapped for slab JC-13 at the FDOT Structures Lab facility to determine the extent and depth of cracks observed on the top of the Prestressed Slab Units (PSU), as can be seen in Figure 10 and Figure 11. The cracks were documented on May 5, 2020. The average depth of the cracks at the top tensile fiber was found to be 1.75 in. deep and the average width was 0.06 in. The cracks started to form approximately a foot away from the end and there was a high density of cracks from 3 ft to 9 ft away from the ends with an average distance in between cracks of 5 in. In the mid-span region, the cracks were approximately at 12 in. spacing.

Figure 10 Cracks Noted at the End of the Slab

Figure 11 Cracks Noted at the Support

Experimental Program

To evaluate each hypothesis mentioned before, destructive tests were required. To study the possibility of excessive force applied to the strands, visual evaluation of the tensile zone of the slab was done as well as the crack opening tests were performed on four slabs (JC-10, JC-11, JC-12, JC-14). To ensure the slabs were constructed with the debonded length documented in the plans, the slabs were cut at two locations after being tested in bending. Finally, to test the concrete properties such as compressive strength and modulus of elasticity, five cylinder cores were extracted from each slab. Additionally, four cylinders were extracted from JC-11 and JC-12 to evaluate the modulus of rupture.

Experimental Procedure

In this section, the procedures for the experimental tests are explained in detail as well as the test setup in the laboratory.

Crack Opening and Ultimate Capacity Tests

The crack opening test was conducted by loading the slabs and analyzing the resulting data to determine the decompression load. With this information, the effective prestress and the prestressing losses in the slabs were calculated.

For these tests, four slabs were tested in bending using a four-point loading until failure. The test setup and gage location can be seen in Figure 13. For these tests, foil strain gages were placed at even increments along the slab with deflection gages at the same locations as shown in Figure 13. The slabs were loaded with a rate of 0.2 kips/sec and the data was recorded at 10 Hz. The test procedure consisted of loading the concrete slab until the first crack was observed at approximately 30 kips, then holding the load to allow the cracks to be marked. The load was removed to install concrete strain gages (CSG) 0.5 in. north and south from the first crack. The slabs were untouched to let the gages cure properly for a few minutes. Finally, the load was applied one more time until the slab reached failure while strain, deflection, and load were recorded.

The effective prestress and load required to crack the slab was estimated by manual calculations. First, the stress due to the prestressing strands was calculated for all of the bonded and debonded strands in the slab using Equation 1, then the stress due to the self-weight of the slab was obtained using Equation 2, and finally, the stress due to an external ultimate load was calculated with the load (P) required to produce the moment due to the load, M_{load}, as an unknown, see Equation 3. Based on stress calculations in the slab, accounting for the stress in the prestressed strands, self-weight, and ultimate load, the expected cracking load was calculated to be 30 kips and the ultimate load was expected to be 59.6 kips, with a deflection of 14 in. Once the test was done and the cracking load was obtained from the crack opening test, moment due to the applied load was substituted in Equation 3 and the effective prestress applied by the strands was determined by setting the sum of stresses equal to zero. The strand stress was compared to the load recorded by the precaster to determine losses.

Equation 1 Stress in the PSU due to Prestressing Strands

$$\sigma_1 = \frac{P_s}{A} + \frac{P_s e}{S_{bottom}}$$

Equation 2 Stress in the PSU due to Self-Weight

$$\sigma_2 = \frac{M_{DL}}{S_{bottom}}$$

Equation 3 Stress in the PSU due to Applied Load

$$\sigma_3 = \frac{M_{load}}{S_{bottom}}$$

Where:

P_s is the load at which the strands were prestressed

A is the transformed cross sectional area

e is the distance from the centroid of the strand to the neutral axis

S_{bottom} is the section modulus measured from the bottom of the slab

M_{DL} is the moment due to dead load

M_{load} is the moment due to the applied load

Concrete Properties

To evaluate the concrete properties such as compressive strength and modulus of elasticity, five (5) cylinders were extracted from each of the four slabs (JC-10, JC-11, JC-12, JC-14) that were tested in bending for the crack opening and ultimate capacity tests. Additionally, to test the tensile strength of the concrete, four (4) cylinders were cored from JC-11 and JC-12, which were from two different concrete pours, for a total of twenty-eight (28) cylinder samples. The cylinders were sent to the FDOT State Material Office in Gainesville, FL to test the compressive strength per ASTM C39 (2018), modulus of elasticity and Poisson's ratio per ASTM C469 (2014), splitting tensile strength per ASTM C496 (2017), and hardened density per ASTM C642 (2013).

Debonded Length Evaluation

Following the ultimate capacity tests, two slabs, JC-11 and JC-12, were saw cut at 3 ft - 10 in. and 7 ft - 10 in. from one end to verify the debonded length of four strands at the bottom layer of the slabs matched the shop drawings. The debonded length is related to the effective prestressing force and therefore the wrong implementation of it could cause either a reduction or an increase in the camber.

Instrumentation

In this section, the instrumentation used on the slabs for the experimental test is explained in detail. Moreover, novel vision-based instrumentation used to determine deflection is explained and details for its use are discussed. The instrumentation for these tests was carefully chosen to obtain the data required to fulfill the project objective. Deflection along the length of the slab was measured using laser deflection gauges and a vision-based Imetrum system. For the strain on the slab, 60mm concrete foil strain gauges were used.

Strain Gauges

Thirteen (13) 60 mm Kyowa strain gauges were installed on the specimen to measure the strain on the concrete. The concrete strain gauges CSG1 to CSG4 were installed after the first crack occurred in the concrete at approximately 30 kips at mid-span. These strain gauges were installed 0.5 in. from the crack with the purpose of measuring the crack opening after reloading the specimen. With this methodology, the decompression load was later determined. The strain was recorded at a rate of 10 Hz and was visually available in real-time. The instrumentation and setup plan can be seen in Figure 13, with the strain gages denoted as CSG#.

Laser Deflection Gauges

Eight (8) MIT Microtrack 3 series LTS 300-200mm laser deflection gages were used along the specimen to determine the deflection at different points. These laser deflection gages were positioned every 7 ft - 8 in. along the beam and two (2) were located at midspan. Deflections were recording at a rate of 10 Hz and were visually available in real-time. The instrumentation layout for the test can be seen in Figure 13, with the deflection gages denoted as D#.

Imetrum

The Imetrum system uses “advance image correlation” that takes images based on patterns in a sequence of frames and calculates displacement and strain. The Imetrum system uses videos and specialized software to measure displacement and strain for research in the areas of structural behavior, mechanical integrity, geotechnical monitoring, and lab and component testing. This system has the potential to replace conventional instrumentation such as LVDTs, tiltmeters, accelerometers, total stations, and seismographs. The system used consisted of a POE Cam-034, 16, 25, and 50mm lenses, and a Wireless Toughpad.

For the crack opening test to determine the deflection of the PSU, the Imetrum system was used with the following setup specifications:

- Two (2) high definition and fixed focal length cameras
- Two (2) 16mm lenses
- Three (3) targets equally spaced on the specimen as shown in Figure 12
- Target dimension of 3.5 in. x 3.5 in.

It is important to note that the Imetrum System is configured in SI Units and therefore, unit conversion was required in the analysis.

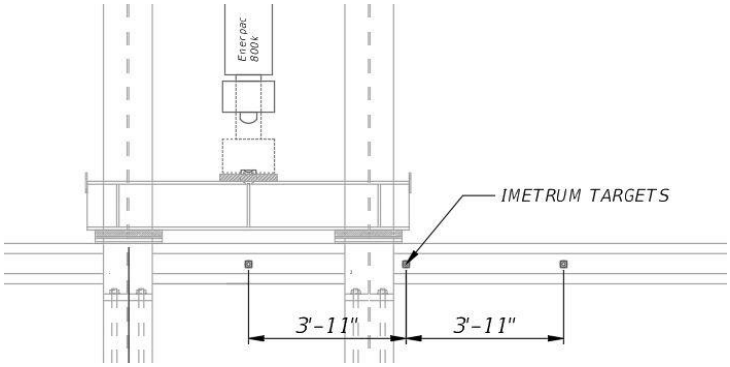

Figure 12 *Target Location*

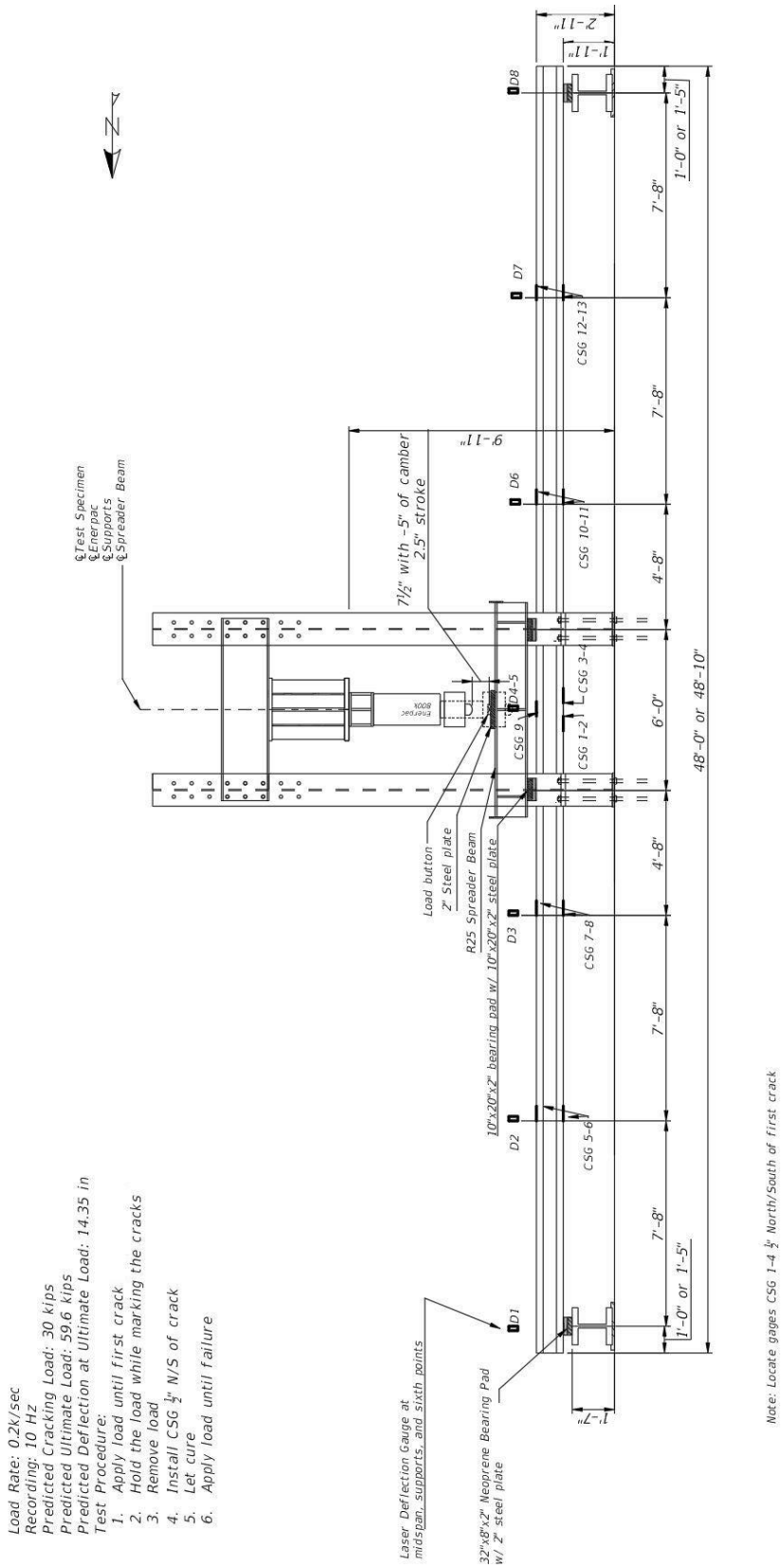

Figure 13 PSU Test Setup

Results

In this section, the results of the experimental testing, such as prestress loss and ultimate capacity are shown, as well as results for the concrete property tests.

Effective Prestress and Loss Determination

Prestress losses were calculated after testing the slabs in four-point bending. Prestress losses are typically estimated using empirical equations, however, for the purpose of this project it is important to accurately determine the prestress loss to properly assess the higher camber in the slabs.

Prestress losses were calculated based on the crack opening test method documented by Pessiki et al. (1996). The method considers the sum of the forces applied to the beam: prestress in the strands (based on design plans), stress due to self-weight of the concrete, and stress due to applied loads (during test). The sum of the stresses at the bottom of the slab is equal to zero at decompression. The effective prestress in the slab can be calculated using the load required to reach decompression (Hamilton, et al., 2017). The effective prestressing force causes compression at the bottom fiber of the slab equal to the tensile stress at the location due to the applied load (decompression load) plus the self-weight. This effective prestressing in the strands is compared to the stress due to the initial tensioning of the strands and then the losses are calculated.

The effective prestress was calculated following the crack opening test method, which consisted of loading the prestressed slab until the first crack was visually defined (approx. 30kips) and applying strain gauges adjacent to the crack. The slab was reloaded again until failure. The strain vs load graph was obtained from strain gauge data and the decompression load was determined. The effective prestress was calculated by summing all the stresses at the bottom fiber of the beam (due to prestress, self-weight, and applied load) to zero, which is the stress at decompression.

The decompression load, defined as the load at which the stress at the extreme tensile fiber transitions from compression to zero, was obtained from the strain vs load graph. This load is represented as the point where the slope changes, as can be seen in Figure 14, in which the strain vs load of SG01 and SG03 for JC-10 are presented. For both gages, the first part of the graph has a linear behavior, however, it is challenging and imprecise to determine the point where the slope changes in this graph. This behavior occurred in all graphs for the four slabs tested.

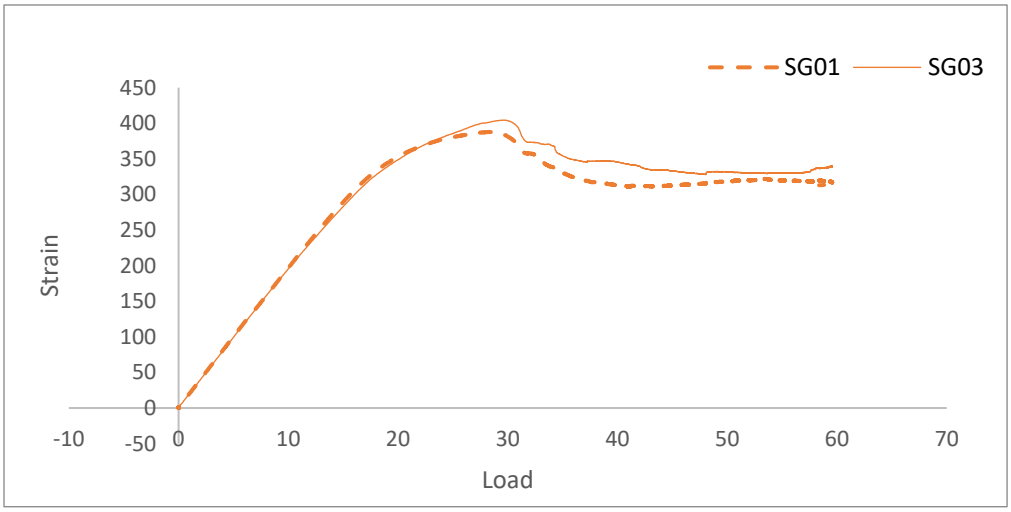

Figure 14 JC-10 Strain vs Load

To accurately determine the decompression load, the slope of both curves, taken at every 5 data points, was graphed versus the load, as shown in Figure 15. A change in the constant region of the slope vs load graph represents a change in slope in the strain vs load graph shown in Figure 14.

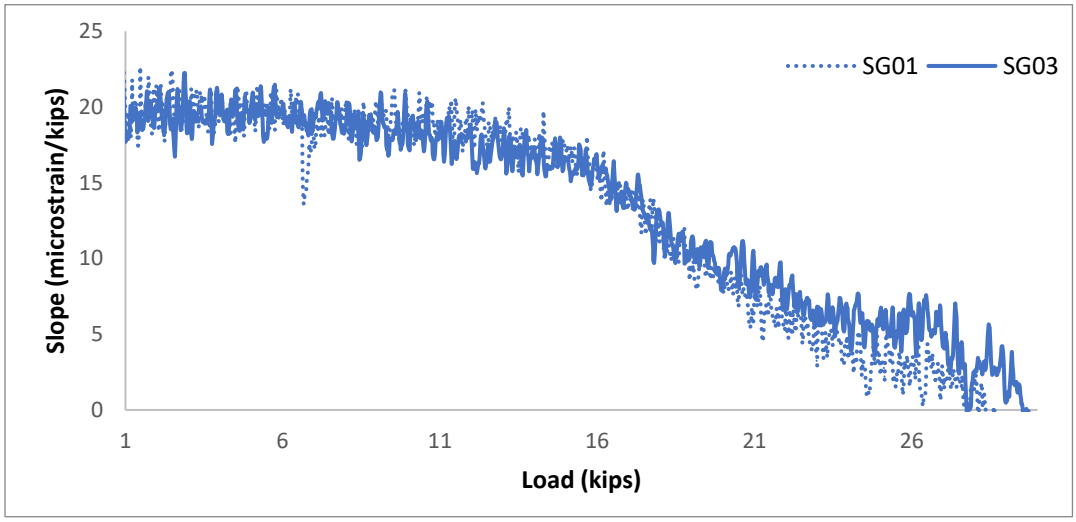

Figure 15 JC-10 Slope vs Load

As can be seen in Figure 15, the first region of the graph has a relatively constant behavior at approximately 20 microstrain/kips, however, the line starts shifting downwards at approximately 16 kips. This change in behavior in the slope vs load graph represents a change of slope in the strain vs load graph, which means the decompression load can be taken as 16 kips for this test. The same methodology was used for the other slabs. In Table 4, the decompression load, effective prestress, and prestress loss of each slab tested can be seen. The effective prestress does not include the stress due to self-weight.

Table 4 Prestress Losses

Slab #	*Decompression Load (kips)*	*Effective Prestress Force (kips)*	*Prestress Loss (%)*
JC-10	16.0	32.4	26.4
JC-11	16.2	32.6	25.9
JC-12	15.8	32.1	26.9
JC-14	15.4	31.7	27.8

The decompression load, effective prestress, and prestress loss, seen in Table 4, were calculated individually for each slab. The decompression load was obtained from the strain vs load graph, as shown in Figure 14, represented as the point where the slope of the graph changes. Once the decompression load was defined, the effective prestress was determined using the crack opening test calculation previously discussed, which considers the stress due to the dead load and the stress due to the applied load. Finally, the prestress loss was obtained comparing the effective stress with the stress to which the slabs were first pretensioned.

Ultimate Capacity Test

The ultimate strength of the slab was evaluated during the four-point bending test, during which the slabs were loaded until failure of the concrete or failure of strands happened. The ultimate capacity test was used to understand the overall behavior of the concrete slab and its response under service load. Four slabs out of the six (JC-10, JC-11, JC-12, JC-14) were loaded to failure. In the four tests, all slabs failed in compression due to concrete failure with no ruptured strands. The results showed consistent behavior among all slabs with an average ultimate load capacity of 59.33 kips for JC-10 and JC-11 cast on Feb 14, 2018, and 55.67 kips for JC-12 and JC-14 cast on Feb 13, 2018, corresponding to a moment capacity of 593.3 kip-ft and 556.7 kip-ft, respectively. The predicted capacity was 486.77 kip-ft, assuming a concrete strength of 6.5 ksi. Slabs JC-10 and JC-11 had a moment capacity 17.95% higher, and JC-12 and JC-14 had a moment capacity 12.56% higher than what was predicted based on the design concrete strength. However, the actual concrete strength exceeded the design strength. The moment capacity calculated using the tested (as-built) compressive strength of the concrete, f_c', of 9605 psi for JC-10 and JC-11, is 589.86 kip-ft. For JC-12 and JC-14, with a tested (as-built) compressive strength, f_c', of 8860 psi, the predicted capacity is 568.08 kip-ft. Comparing the calculated moment capacity using as-built compressive strength with the moment capacity obtained from the four point bending test the actual capacity is 0.56% higher than would be predicted for JC-10 and JC-11 and 2% lower than would be predicted for JC-12 and JC-14. This shows that the capacity of slabs was close to what would be predicted using the tested concrete strength.

Imetrum System vs Laser Deflection Gauges

Deflection of the slabs during the four-point bending test was measured using two instrument systems, conventional laser deflection gages and the vision-based Imetrum system (for JC-12 and JC-10 only). The results of these two measurement methods were analyzed individually and compared.

In Figure 16, the graph of the deflection obtained from the laser deflection gage and the Imetrum system at midspan for the JC-12 slab are shown. In solid line is the Imetrum system readings and in dashed line is the laser deflection gage readings. As can be observed in Figure 16, both readings are almost identical with a final deflection at midspan of -11.65 in. for the Imetrum system and -11.84 in. for the laser deflection gages. The percentage error of these two readings is 1.6% at maximum deflection.

For the deflection evaluation at midspan of slab JC-10, Figure 17 shows the comparison of the laser deflection readings and the Imetrum system. As can be seen in Figure 17, both results were very consistent, however, the maximum deflection in the Imetrum system was less than what was recorded with the laser deflection gauge. The maximum deflection recorded using the Imetrum system was -12.67 in. and using laser deflection gauges, it was -13.19 in. Moreover, recorded data from the Imetrum system lasted 571 seconds and recorded data from the laser deflection gages was 600 seconds. The difference in time and deflection measurement was due to the beam deflecting below the field of view of the Imetrum system.

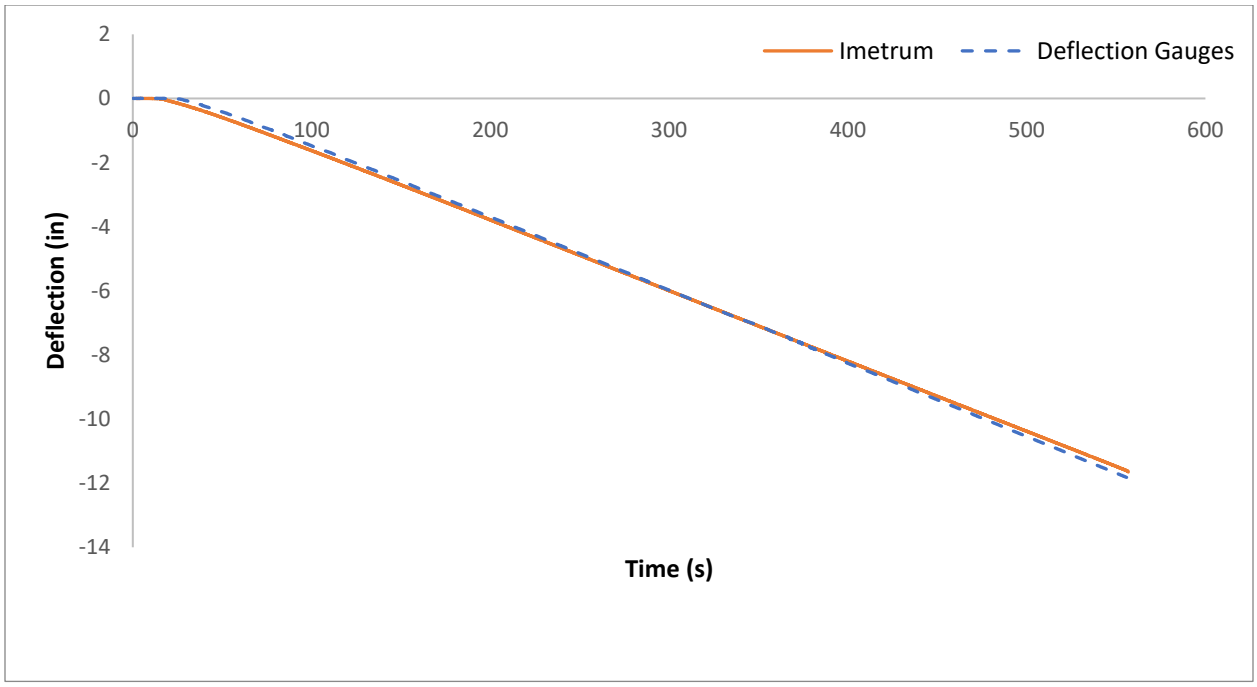

Figure 16 Deflection Gage and Imetrum System Readings at Midspan for JC-12

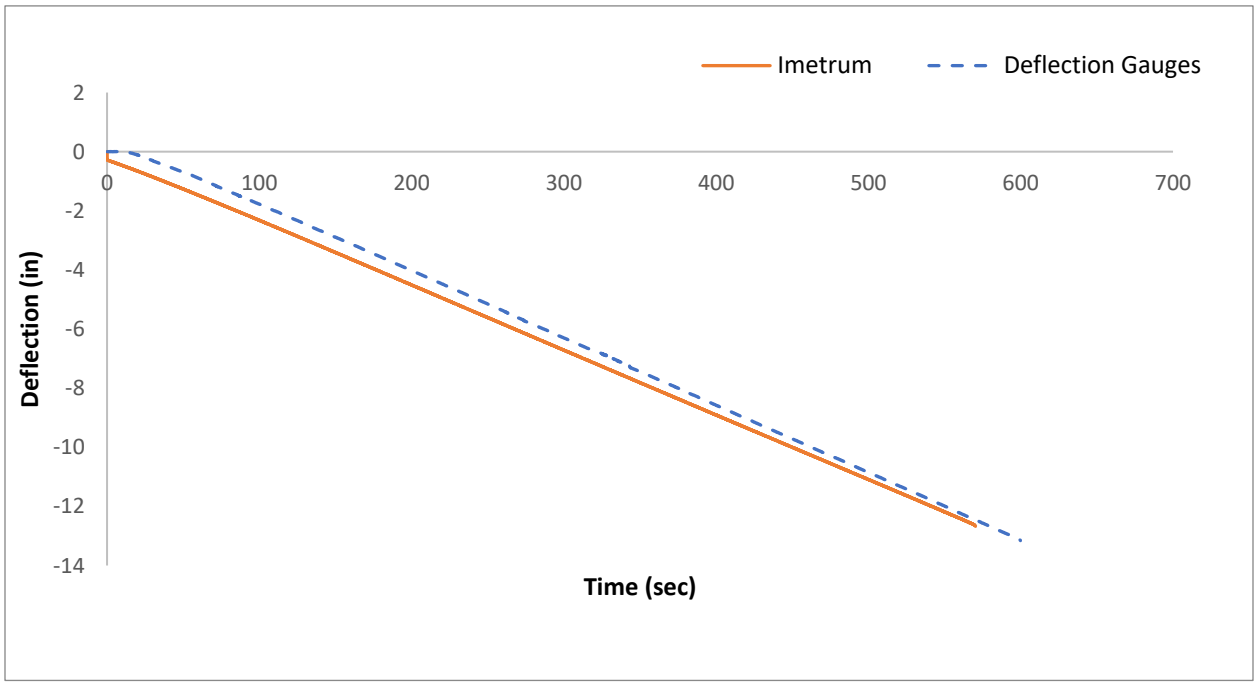

Figure 17 Deflection Gage and Imetrum System Readings at Midspan for JC-10

Concrete Properties

The core cylinders were tested at the FDOT State Materials Office in Gainesville, FL on March, 2020 and the results of all tests were sent to the FDOT Structures Laboratory in Tallahassee, FL. The concrete properties results are shown in this section.

Immersed Volume

The concrete unit density was determined for the cores extracted from slabs JC-10, JC-11, JC-12 and JC-14. The density was measured following ASTM C642 (2013), which requires oven-drying the specimen to calculate the dry mass, followed by immersing the specimen in water to calculate the mass in water, then boiling the specimen for 5 hours to calculate the boiled mass, and finally, suspending the specimen on a wire to determine the apparent mass in water. After that process, the actual density of the concrete is determined. For slabs JC-10, JC-11, JC-12 and JC-14, the average concrete density was 136.2 pcf with a standard deviation of 0.66.

The tested density of the concrete is considered in the low range for normal reinforced concrete which is defined as concrete with a unit weight between 135 and 155 pcf according to AASHTO (2017). A design unit weight of 145 pcf is recommended for use by the FDOT Structures Design Guidelines (2015). The tested density was used for the calculation of the camber in the following sections.

Compressive Strength

The compressive strength of the concrete was measured on March 22, 2020 for the four slabs tested following ASTM C-39 (2018). Within these slabs, JC-10 and JC-11 were cast on Feb 14, 2018 and JC-12 and JC-14 were cast Feb 13, 2018. The result for this test can be seen in Table 5. As shown in Table 5, slab JC-10 had the highest compressive strength whereas JC-14, cast on a different day, had a compressive strength of almost 2000 psi less.

Table 5 Compressive Strength

Cast Day	*February 14, 2018*		*February 13, 2018*	
Slab ID	JC-10	JC-11	JC-12	JC-14
Compressive Strength (psi)	10019	9190	9608	8111

Modulus of Elasticity

The modulus of elasticity was tested following ASTM C-469 (2014). The results show that the average modulus of elasticity for the slabs cast on Feb 14, 2018 was 5223 ksi whereas the slabs cast on Feb 13, 2018 had a lower average modulus of elasticity of 5152 ksi. There was not a significant difference in the modulus of elasticity within these four slabs. The results show that the slabs cast on Feb 14 had a slightly stiffer concrete compared to the slabs cast on Feb 13.

Splitting Tensile Strength

The tensile strength was evaluated from two slabs cast on different days, JC-11 and JC-12. This test was done to evaluate the tensile properties of the concrete following ASTM C-496 splitting tensile test (2017). The results show very similar values for both slabs. For JC-11, 560 psi and for JC-12, 568.75 psi. These results show consistency in the strength of the concrete since JC-12 had a higher compressive strength and therefore a higher tensile strength.

Debonded Length

An inaccurate debonded length of the strands was a hypothesis that could explain the excess camber of the slabs. To evaluate this hypothesis, slabs JC-11 and JC-12 were saw cut, after being tested in bending, at 3 ft -10 in. and 7 ft -10 in. from the end to visually confirm the presence of debonding sheathing, as can be seen in Figure 18 and Figure 19.

Figure 18 Debonded Strands

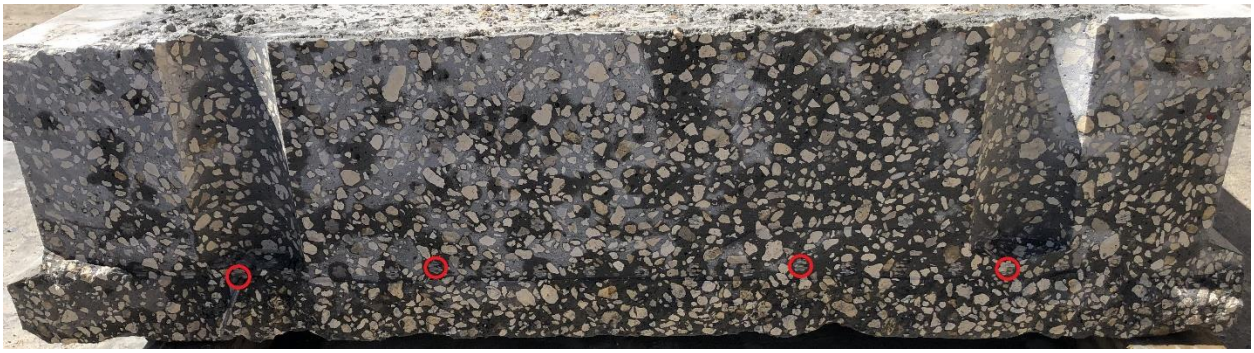

Figure 19 Location of Debonded Strands

In Figure 18 , the debonded strands are circled in red. The strand closer to the edge is debonded 8 ft as stated in the shop drawings and the strand closer to the middle of the cross-section is debonded 4 ft as stated in the shop drawings. In Figure 19, the entire cross-section of the slab can be seen with the locations of the four debonded stands, both 4 ft and 8 ft from the ends, circled in red. Visual observations of the cut slabs indicate the slabs were debonded as planned.

Analytical Evaluation

In this section, the results obtained from the analytical evaluations of excessive camber in the six rejected slabs are shown. Three different methods of calculating camber were used. The results obtained in these methods were compared to the predicted camber recorded on the plans and the actual camber at the time of slab rejection.

Camber Calculation

Before continuing with the camber calculation, it was important to study the methodology used by the Engineer of Record (EOR) to design and estimate the camber in the concrete slabs. The camber calculated by the EOR was done using the FDOT LRFD Prestressed Beam Program version 3.33 (2014). Based on the information provided by the EOR, the design strength of the concrete at release was 5 ksi and the density of the concrete was 0.145 kip/ft^3. The research team re-designed the beam using the same properties and the FDOT LRFD Prestressed Beam Program version 3.33 and obtained the same predicted camber.

The original design by the EOR was controlled by ultimate moment strength and long-term camber. The minimum capacity ratio for the strength limit state moment was 1.04 at approximately mid-span. The long-term camber, which is required by the FDOT Structures Design Guidelines (2015) to be positive at the end of construction after all non-composite and composite loads have been added, was predicted by the EOR to be only 0.04 in. In contrast, the minimum capacity ratio for long-term service stresses was 1.12.

For comparison, the research team estimated camber using the design information and the latest version of the FDOT LRFD Prestressed Beam program, version 5.2 (2018). The results obtained are compared to the original design results in Table 6.

Table 6 Design Camber Comparison

	EOR's Design Program version 3.33	*Research Team's Estimate Program version 5.2*
Modulus of Elasticity (initial)	3663 ksi	4291 ksi
Camber at release	0.6 in	0.59 in
Camber at 90 days	1.29 in	1.55 in

As can be seen in Table 6, although the same concrete properties were used for both designs, the initial modulus of elasticity and the prediction for 90 day camber differed. There were two revisions to the FDOT LRFD Prestressed Beam program which account for the differences. The modulus of elasticity obtained from the EOR's design was based on the AASHTO LRFD Bridge Design Specifications, 7th edition (2016), in which the calculation of the initial modulus of elasticity depends on the aggregate factor. According to the 2015 FDOT Structures Design Guidelines (2015), the aggregate factor in Florida was 0.9. In the new version of the FDOT LRFD Prestressed Beam program, the calculation of the modulus of elasticity is based on the AASHTO LRFD Bridge Design Specifications, 8th edition (2017), where the initial modulus of elasticity depends on the weight and the compressive strength of the concrete. This change in the guidelines explains the different predictions in the modulus of elasticity. Additional differences in camber prediction are due to a change in the creep coefficients. In version 3.33 of the program, the time dependent equation for creep coefficient was based on AASHTO LRFD Bridge Design Specifications, 1st edition (1994).

According to commentary, the equation in the code is based on the recommendation of ACI Committee 209 and Collins and Mitchell (1991). The time dependent equation for creep coefficient was revised in the 4th edition of the AASHTO LRFD Bridge Design Specifications (2007), and the revised equation is what is used in version 5.2 of the FDOT LRFD Prestressed Beam program. According to AASHTO commentary, the equation is again based on recommendations from ACI Committee 209 and additional recently published data.

The initial modulus of elasticity has an influence on the final camber of the concrete slab. Since this property is not commonly measured during construction projects, there is no record of it and the initial modulus of elasticity of the concrete cannot be directly measured once the concrete has matured. For this reason, methods and guidelines were evaluated to estimate the initial modulus of elasticity based on the tested modulus of elasticity obtained from the cylinders extracted from the slabs. A methodology was used based on the research conducted by Singh et al. (2013) titled *Effect of a Time Dependent Concrete Modulus of Elasticity on Prestress Losses in Bridge Girder*. In this research, a method based on the CEB-FIP model code uses the long-term modulus of elasticity to predict the initial modulus of elasticity of the concrete. Using the method based on CEB-FIP model code and the average concrete modulus of elasticity measured at an age of 766 days (5187 ksi), the 28 day concrete modulus of elasticity was estimated to be 4690 ksi and the initial (2 day) modulus of elasticity was estimated to be 3330 ksi. For comparison, the 28 day modulus of elasticity was calculated using AASHTO LRFD 8th edition and it was determined to be 4682 ksi, which is very close to the prediction using CEB-FIP.

To continue investigating the high camber of the rejected slabs, camber predictions were done using the tested properties of the concrete. Specific properties used were a concrete unit density of 136 pcf, concrete strength at release of 5400 psi, 28 day concrete strength of 8365 psi, initial concrete modulus of elasticity of 3330 ksi and 28 day concrete modulus of elasticity of 4690 ksi. Using transformed properties of the slab, the analytically predicted camber was calculated using two different methods. The first was a manual method, based on PCI guidelines using PCI multipliers (2004). The second method used was the FDOT LRFD Prestressed Beam Program, version 5.2 (2018). The program calculates the predicted slab camber based on FDOT standards of shape and dimensions. This program provides an estimated calculation of the long-term camber of the slab using transformed properties.

The calculations based on the PCI multiplier method were done following the PCI Design Handbook, Sixth Edition (2010). The PCI multipliers used at erection were 1.85 for downward deflection due to self-weight and 1.80 for camber due to prestress. The deflection equations used were:

Equation 4 Camber Deflection due to Self-Weight

$$\Delta_{sw} = \frac{5wl^4}{384E_{ci}I}$$

Equation 5 Camber Deflection due to Prestressing

$$\Delta_{ps} = \frac{P_i e l^2}{8E_{ci}I}$$

Where:

w is the self-weight of the concrete slab beam

l is the span length of the beam

E_{ci} is the initial concrete modulus of elasticity

I is the transformed moment of inertia

P_i is the initial prestressing force

e is the eccentricity of the prestressing force

The first method using the PCI guidelines and multiplier method produced a predicted camber at erection of 3.15 in. The second method using the FDOT LRFD Prestressed Beam Program version 5.2, produced a predicted 90 day camber of 2.43 in. Compared to the readings taken at the precast facility, which averaged 4.29 in at 90 days, a significant difference is still observed. The difference is 1.14 in. if the PCI method is used and 1.86 in. if the FDOT program is used. The difference in as-built concrete properties alone does not fully explain the unusually high camber in the subject prestressed slab units.

Stress Release

Compressive stresses at release were manually calculated using the tested properties of the concrete and were compared to the limits allowed by the AASHTO LRFD Bridge Design Specifications. As previously mentioned, the EOR designed the slabs based on AASHTO LRFD Bridge Design Specifications 7th edition (2016), which allows compressive stress at the bottom fiber of the slab to be up to $0.6f_c'$, whereas AASHTO LRFD Bridge Design Specifications 8th edition (2017), which is the current edition, allows $0.65f_c'$. When calculating the stress at release in the rejected slabs based on tested properties, it was noted that the stresses at the bottom fiber exceeded the stress limit for the applicable code at the time of design, AASHTO LRFD Bridge Design Specifications, 7th edition, by 2.9%. The bottom fiber stress at release can be seen in Figure 20. The $0.6f_c'$ limit was exceeded but the $0.65f_c'$ limit was not. Although the compressive stress was high compared to the AASHTO LRFD Bridge Design Specifications, it was less than the $0.7f_c'$ limit recommended by Dolan and Krohn (2007) for avoiding excess camber.

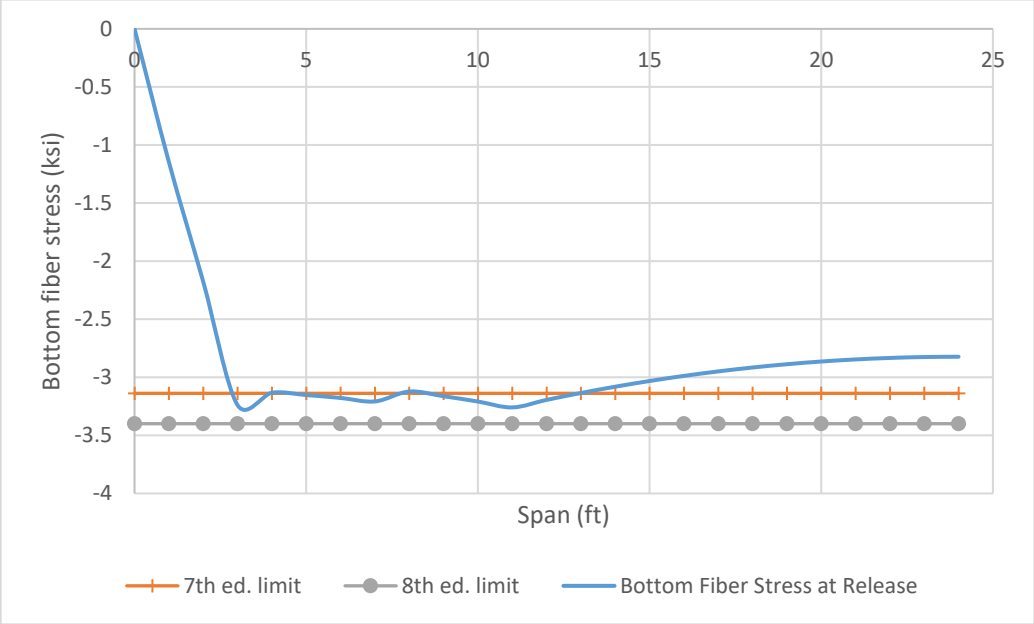

Figure 20 Bottom Fiber Compressive Stress at Release, 4 ft Wide Units

All of the 5 ft wide prestressed slab units, which were built for this bridge project at the same time as the 4 ft wide prestressed slab units studied herein, had an acceptable level of camber. All of those 5 foot wide units would have had bottom fiber stress exceeding the $0.6f_c'$ limit as well, as shown in Figure 21, if concrete with the same unit weight and strength was used. The magnitude of exceedance is similar, however, the length of the beam for which the stress limit is exceeded is shorter.

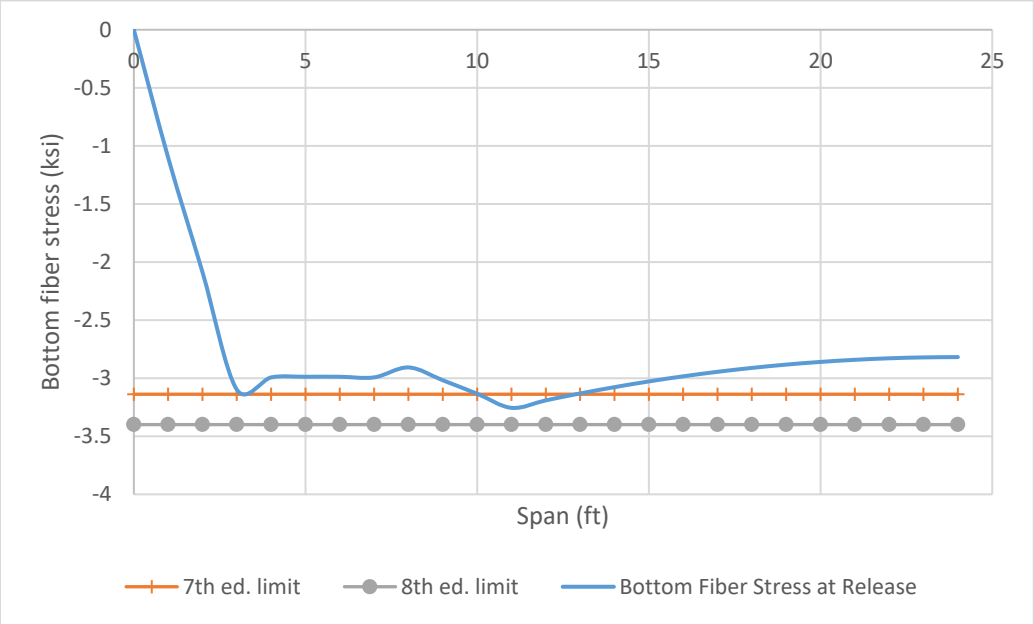

Figure 21 Bottom Fiber Compressive Stress at Release, 5 ft Wide Units

Microcrack Evaluation

Cracks evident in the top of one of the slabs indicate that the moment of inertia resisting upward movement (camber) of the slabs may be reduced compared to the uncracked section which is generally assumed for design. It was attempted to determine an effective cracked moment of inertia which would have produced the observed average 4.29 in of camber noted by the precaster. The PCI multiplier method was used, with the initial modulus of elasticity for concrete and gross and transformed properties. However, with a reduced moment of inertia, the deflection due to self-weight overcame the camber due to prestressing. A reduced moment of inertia due to cracking in the top fiber of the beam does not explain the unusually high camber.

Discussion

From the results obtained in the research, it was observed that the as-built 28 day concrete strength exceeded the design value by more than 2,300 psi. However, the tested weight of the concrete, 0.136 kcf, was lower than expected, 0.145 kcf. In fact, the tested weight of the concrete falls very close to being categorized as a lightweight concrete, which was not the type of concrete intended for the design of the slabs in this project. The weight of the concrete plays an important role in the design and the final camber of the slabs. The weight of the concrete affects the prediction of the modulus of elasticity, which defines the stiffness of the concrete slab. The first days after the release of the strands are the most critical days for the camber of the concrete member, which means that the initial modulus of elasticity is an important factor for the prediction of camber. A lower weight concrete could have a smaller initial modulus of elasticity and therefore a less stiff member. In this research the exact initial modulus of elasticity was unknown, therefore, the initial modulus of elasticity was estimated. The 28-day modulus of elasticity was estimated to be 4690 ksi, which was close to, but higher than, the design value of 4176 ksi. So, the lighter weight concrete noted in the slabs contributes to, but is not enough to cause such a high camber.

Other causes were investigated that could explain high camber such as high stress release and microcracking at the tensile fiber of the slabs. The compressive stress at release was calculated using the as-built properties of the concrete, which exceeded the compressive stress limit of $0.6f_c'$ by approximately 2.9%, primarily due to the concrete having a lighter weight than designed. Some literature indicates that high initial compressive stress can result in microcracking, although the literature notes that is a problem above a stress limit of $0.7f_c'$, which was not exceeded for these slabs. The tensile zone of the slab was visually analyzed, and a high number of cracks were found and mapped. The average depth of the observed cracks was 1.75 in. spaced differently throughout the slab but with higher density in the range of 4ft to 10ft away from the ends. The high volume of cracks at the tensile fiber of the slab may have led to a reduction of the moment of inertia but does not explain the excess camber experienced in the slabs. The exact reason of the cracks at the tensile fiber of the slab is unknown, however, it could be a combination of shrinkage, excess of compressive stress at release, and low concrete weight.

Moreover, the effective prestress on the slabs was obtained through the crack opening test and the results indicated a very high average of 27% prestress losses in the four slabs tested after 2 years of being constructed. Losses of 14% were predicted in the design calculations. Additionally, a four-point test was conducted until failure to evaluate the ultimate capacity of the slabs. The moment ultimate capacity was also predicted using design concrete properties and as-built concrete properties. The analytical prediction based on design strength was lower than the tested moment ultimate capacity by an average of 15%. The analytical prediction based on as-built concrete strength was approximately equal to the tested moment ultimate capacity. This means that the slabs exceeded the design capacity and if the beams had been installed in the bridge with a deck cast on it, the concrete section would have produced sufficient capacity to carry design loads.

Conclusions

The following conclusions can be drawn from this research:

- The unit density of the concrete used to construct the Prestressed Slab Units investigated in this study was lower (7%) than the concrete unit density assumed for design.
- The prestress losses in all of the tested slabs were higher than expected.
- The density of the concrete, 136 pcf, affects the initial modulus of elasticity and self-weight, which means that the initial camber was higher than predicted.
- Based on measured material properties, the compressive stresses were higher than the limit allowed by the AASHTO LRFD Bridge Design Specifications applicable at the time these slabs were designed, but lower than current code limits. The primary reason that compressive stresses exceeded the limits allowed by the applicable code at the time of design was the light unit weight of the concrete.
- High compressive stresses at the transfer of prestressing force have been associated with excess camber and microcracking, but the stress analytically back-calculated did not exceed the limit presented in the literature above which excess camber and microcracking become problematic.
- The presence of cracks in the top of the Prestressed Slab Units indicates a reduced moment of inertia for resisting upward movement (camber), but the reduced moment of inertia does not explain the excess camber.
- The reason for cracking is unknown, but could be due to shrinkage, high compressive stresses at release, excess of compressive stress at release or a combination of the three.
- The predicted ultimate capacity of the slab was calculated using both design and as-built concrete properties. Compared to the tested ultimate capacity of the slabs, the actual capacity was at least 12.5% higher than the capacity predicted using design concrete properties but, on average, 1% lower than what would be predicted using as-built concrete properties.
- The Prestressed Slab Units tested would have had sufficient capacity to carry traffic based on design demands, but the camber was in excess of what would be acceptable for geometric concerns and design accommodating the excessive overlay would have needed investigation.

Bibliography

ACI Committee 209. (2015). *Creep and Shrinkage in Concrete.* Denver: ACI.

American Association of State and Highway Transportation Officials. (2007). *AASHTO LRFD Bridge Design Specifications 4th edition.* Washington, D.C.

American Association of State Highway and Transportation Officials. (1994). *AASHTO LRFD Bridge Design Specifications, 1st Edition.* Washington, D.C.

American Association of State Highway and Transportation Officials. (2016). *AASHTO LRFD Bridge Design Specifications 7th Edition.* Washington, D.C.

American Association of State Highway and Transportation Officials. (2017). *AASHTO LRFD Bridge Design Specifications 8th Edition.* Washington, D.C.

ASTM. (2013). *ASTM C642: Standard Test Method for Density, Absorption, and Voids in Hardened Concrete.* West Conshohocken.

ASTM. (2013). *ASTM C642-13: Standard Test Method for Density, Absorption, and Voids in Hardened Concrete.* West Conshohocken.

ASTM. (2014). ASTM C469/ C469M-14. Standard Test Method for Static Modulus of Elasticity and Poisson's Ratio of Concrete in Compression. West Conshohocken, PA.

ASTM. (2017). *ASTM C496/ C496M-17: Standard Test Method for Splitting Tensile Strength of Cylindrical Concrete Specimens.* West Conshohocken.

ASTM. (2018). ASTM C39. Standard Test Method for Compressive Strength of Cylindrical Concrete Specimens. West Conshohocken, PA.

Azizinamini, A., Keeler, B. J., Rohde, J., & Mehrabi, A. B. (1996). Application of a New Nondestructive Evaluation Technique to a 25-Year-Old Prestressed Concrete Girder. *PCI*, 14.

Castro , A., Kreger, M. E., Bayrak, O., Breen, J. E., & Wood, S. L. (2004). *Allowable Design Release Stresses for Pretensioned Concrete Beams.* Austin: Texas Department of Transportation.

Collins, M. P., & Mitchell, D. (1991). *Prestressed Concrete Structures.* Englewood Cliffs, NJ: Prentice Hall.

Cook, R. A., Bloomquist, D., Sanek, J. E., & Ansley, M. H. (2005). *Field Verification of Camber Estimates for Pressted Concrete Bridge Girders.* Tallahassee: Florida Department of Transportation.

Dolan, C. W., & Krohn, J. J. (2007). *A Case for Increasing The Allowable Compressive Release Stress for Prestressed Concrete.* PCI Journal.

Federal Highway Administration. (n.d.). *Lightweight Concrete: Mechanical Properties.* McLean: U.S. Department of Transportation.

Florida Department of Transportation. (2014). FDOT LRFD Prestressed Beam Program v3.33. Tallahassee.

Florida Department of Transportation. (2015). *Structural Design Guidelines Vol. 1.* Tallahassee: FDOT.

Florida Department of Transportation. (2018). FDOT LRFD Prestressed Beam Program v5.2. Tallahassee.

Florida Highway Administration. (n.d.). *Comprehensive Design Example for Prestressed Concrete (PSC) Girder Superstructure Bridge.* FHWA.

Hamilton, H. R., & O'Neill, C. (2009). *Determination of Service Stresses in Pretensioned Beams.* Gainesville: University of Florida.

Hamilton, H. R., Rice, J. A., Abdullah, A. M., Bhatia, R., Brenkus, N., & Skelton, D. (2017). *Replaceable Unbonded Tendons for Post-Tensioned Bridges.* Gainesville: University of Florida.

Martí-Vargas, J., Garcia-Taengua, E., & Caro, L. (2014). *Measuring specific parameters in pretensioned concrete members using a single testing technique.* Valencia: ICITECH, Institute of Concrete Science and Technology.

Nawy, E. G. (2005). *Prestressed Concrete: A Fundamental Approach.* New York: Prentice Hall.

Nilson, A. H., Darwin, D., & Dolan, C. W. (2004). *Design of Concrete Structures.* New York: McGraw Hill Higher Education.

PCI. (2004). *PCI Design Handbook Sixth Edition.*

PCI. (2010). *PCI Design Handbook.* Chicago: PCI.

Pessiki, S., Kaczinski, M., & Wescott, H. H. (1996). Evaluation of Effective Prestress Force in 28-Year-Old Prestressed Concrete Bridge beams. *PCI*, 12.

Singh, B. P., Yazdani, N., & Ramirez, G. (2013). Effect of a Time Dependent Concrete Modulus of Elasticity on Prestress Losses in Bridge Girders. *International Journal of Concrete Structures and Material, 7*(3), 183-191.

Storm, T. K., Rizkalla, S. H., & Zia, P. Z. (2013). Effects of Production Practice on Camber of Prestressed Concrete Bridge Girders. *PCI*, 16.

Tadros, M. K., Al-Omaishi,, N., Seguirant, S. J., & Gallt, J. G. (2003). *Prestress Losses in Pretensioned High-Strength Concrete Bridge Girders.* Washington, D.C.: Transportation Research Board.

Yazdani, N., Mtenga, P., & Richardson, N. (1999). Camber Variation in Precast Bridge Girders. 6.